SCIENCE CHINA
Technological Sciences

Special Topic: Multimodal Hyperspectral Remote Sensing Technology
•Article•

April 2022 Vol.65 No.4: 793–801
https://doi.org/10.1007/s11431-021-1989-9

Self-supervised learning-based oil spill detection of hyperspectral images

DUAN PuHong[1,2], XIE ZhuoJun[1,2], KANG XuDong[1,2*] & LI ShuTao[1,2]

[1] *College of Electrical and Information Engineering, Hunan University, Changsha 410082, China;*
[2] *Key Laboratory of Visual Perception and Artificial Intelligence of Hunan Province, Changsha 410082, China*

Received September 13, 2021; accepted December 22, 2021; published online March 22, 2022

Oil spill monitoring in remote sensing field has become a very popular technology to detect the spatial distribution of polluted regions. However, previous studies mainly focus on the supervised detection technologies, which requires a large number of high-quality training set. To solve this problem, we propose a self-supervised learning method to learn the deep neural network from unlabelled hyperspectral data for oil spill detection, which consists of three parts: data augmentation, unsupervised deep feature learning, and oil spill detection network. First, the original image is augmented with spectral and spatial transformation to improve robustness of the self-supervised model. Then, the deep neural networks are trained on the augmented data without label information to produce the high-level semantic features. Finally, the pre-trained parameters are transferred to establish a neural network classifier to obtain the detection result, where a contrastive loss is developed to fine-tune the learned parameters so as to improve the generalization ability of the proposed method. Experiments performed on ten oil spill datasets reveal that the proposed method obtains promising detection performance with respect to other state-of-the-art hyperspectral detection approaches.

hyperspectral image, self-supervised learning, data augmentation, oil spill detection, contrastive loss

Citation: Duan P H, Xie Z J, Kang X D, et al. Self-supervised learning-based oil spill detection of hyperspectral images. Sci China Tech Sci, 2022, 65: 793–801, https://doi.org/10.1007/s11431-021-1989-9

1 Introduction

Recently, the increasing frequency of oil leakage leads to massive amount of crude oil being spilled into the ocean, which seriously threatens the living environment of marine creatures and human beings [1]. In 2010, the Deepwater Horizon drilling platform situated in the Gulf of Mexico has suffered from explosion, which leads to 4.9 million barrels of crude oil discharging into the Gulf. A diversity of coastal species has been contaminated from the oil spill. It was estimated that up to 65000 imperilled turtles had died during 2010 alone, mostly as a result of oil contamination. In 2011, the Penglai 19-3 oil field witnessed oil spill accident located in Bohai Bay, which causes more than 7 barrels of oil leaking into the Bohai Bay, and approximately 6200 square kilometres of ocean is polluted. If the spilled oils cannot be cleaned timely, the oil film is easily washed to the coast by the waves, which exerts profound negative effects, such as fires, coastal aquaculture, and salt production. As a result, it is necessary to rapidly detect the spatial distribution of oil spill on the ocean surface, facilitating oil spill clean-up and government decision-making.

Remote sensing has become an important technology in detecting oil spill regions. Compared with other remote sensing data, hyperspectral images not only provide the detailed spatial information, and record the finer spectral information. This unique characteristic makes it more effective to distinguish the oil spill and seawater [2–8]. In the last

*Corresponding author (email: xudong_kang@163.com)

decades, many oil spill detection methods have been investigated [9–14], which can be roughly divided into four classes: spectral classifier-based methods, spectral matching-based methods, hand-crafted feature extraction methods and deep learning models.

In the complicated ocean surface, the captured hyperspectral images are usually corrupted by multiple degradation factors, such as image noise, sun glints, and shadows, which seriously affect the following detection performance. To alleviate this issue, some scholars developed hyperspectral image restoration approaches, and applied the spectral classifiers on the reconstructed data for oil spill detection. The spectral classifiers mainly include support vector machine (SVM), random forest (RF), and multinomial logistic regression (MLR). For example, Yang et al. [9] applied SVM classifier on the recovered hyperspectral image to achieve oil spill detection, in which the recovered image was obtained by performing wavelet transform and three different filters on the original image to remove image noise and sun glints. In ref. [10], the RF classifier was conducted on the selected spectral indices to obtain oil pollution maps. In ref. [11], a texture-aware total variation method was proposed to eliminate the sun glints of original images, and the SVM classifier was utilized to detect the oil spill on the sea surface.

Spectral matching-based methods aim to measure the spectral similarity between the given spectrum and all candidate spectra. For instance, Liu et al. [12] proposed a novel spectral curve shape matching method, in which the first-order and second-order spectral derivatives were combined to measure the affinity between the reference spectrum and the observed spectrum. In ref. [13], a conventional adaptive cosine estimator method was proposed to automatically detect the oil spill areas.

Hand-crafted feature extraction methods are designed to extract the shallow spatial features from original images followed by a spectral classifier, which is beneficial for removing image noise and shadows. In the past decades, researchers mainly focus on the development of oil spill detection with traditional machine learning technologies [14–16]. For example, Song et al. [14] applied wavelet transform to increase the difference of spectral characteristic between thin and thick oil film, where the low-frequency coefficients were taken as the sensitive bands for following task. Liu et al. [15] studied a decision tree framework for oil spill detection, in which the minimum noise fraction was used as feature extractor. Song et al. [16] used an active contour model to characterize the spectral-spatial features of the input, which was helpful for reducing the interference of sun glints and shadows on the ocean surface.

Furthermore, many deep learning models have also been applied for oil spill detection of hyperspectral images in recent several years [17–21]. These methods can extract deep semantic features of original images, which show more robust detection performance. For example, Wang et al. [17] developed a spectral-spatial integrated network for marine oil spill detection, where the 1D and 2D convolutional neural network (CNN) models were used to extract the spectral-spatial features. Zhu et al. [18] investigated oil film classification performance of several deep learning models, including back propagation (BP) neural network, stacked autoencoders (SAEs), AlexNet, and VGGNet. Yang et al. [19] proposed a multi-scale deep CNNs for sea oil spill detection, in which the multi-scale features were constructed by using wavelet transform.

These methods mentioned above can achieve satisfactory detection performance when the number of training samples is sufficient. However, the collection of training set is time-consuming and expensive cost. In this situation, these oil spill detection approaches tend to be over-fitting and produce poor generalization performance with limited labelled training set.

To address this problem, we propose a self-supervised learning method for oil spill detection of hyperspectral images. The proposed method gives a new perspective on unsupervised deep feature characterization of hyperspectral images, in which a queue of feature vectors is generated and a momentum encoder is introduced to update the queue. To this end, first, a spectral and spatial transformation-based augmentation method is exploited to increase robustness of the proposed method. Then, a CNN encoder is learned to extract the deep embedding features by minimizing the normalized similarity between the features extracted from the input image and its augmented correspondents. Finally, the pre-trained CNN encoder is transferred into detecting oil spill regions. With the goal of verifying the proposed approach, the proposed method is compared with different object detection techniques in hyperspectral image community on a benchmark dataset. Experimental results show that the proposed method can obtain superior performance for oil spill detection without any label information. The main contributions of this work are as follows.

(1) We propose a self-supervised representation learning with similarity loss for oil spill detection of hyperspectral images. To the best of our knowledge, this is the first attempt to achieve hyperspectral oil spill detection with self-supervised representation learning model. The high-level semantic features under complex background are extracted without labelled samples.

(2) We develop a spectral similarity-based contrastive loss to enhance the discrimination between different objects and alleviate the spectral variability of the same object, which is helpful for increasing the transfer capability of the proposed method.

(3) Experiments performed on a benchmark hyperspectral dataset demonstrate that the proposed method obtains promising detection performance with respect to other su-

pervised and unsupervised detection approaches.

This work is organized as follows. In Sect. 2, we mainly describe the detailed steps of the proposed method for hyperspectral oil spill detection. In Sect. 3, the experimental results are presented and discussed. In Sect. 4, several core conclusions of this work are given.

2 Proposed method

In this section, we describe the detailed steps of the proposed model for hyperspectral oil spill detection, which mainly consists of three steps: data augmentation, self-supervised feature learning, and oil spill detection network. Figure 1 depicts the schematic of the proposed method.

2.1 Data augmentation

Data augmentation is an important technique for deep learning models, which is able to avoid model overfitting and enhance the robustness of the model. Currently many augmentation techniques have been widely applied in image processing [22–25], such as rotation, flip, and mirror. In this work, considering the 3D characteristic of hyperspectral image, a spectral and spatial image transformation-based data augmentation technique is adopted to increase the diversity of training data, including spatial mirror, spatial rotation, spectral mirror, and random noise. The details of these operations are shown in Figure 2. More specifically, let $\mathbf{I}$ be the input data, we first perform a horizontal mirror operation on the input data $\mathbf{I}$ to obtain the spatial mirroring data. Then, the spatial mirroring data are added random noise to yield noisy data $\tilde{\mathbf{I}}$. Next, a rotation operation is conducted on the noisy data $\tilde{\mathbf{I}}$ along with the horizontal dimension to obtain horizontal rotated data $\{\tilde{\mathbf{I}}^{\theta} \mid \theta \in \Theta\}$, where $\Theta = \{90^0 \cdot t \mid t \in [0,1,2,3]\}$denotes the rotation degree set and $\tilde{\mathbf{I}}^{\theta}$ is the augmented image of $\tilde{\mathbf{I}}$ rotated by θ degree. Finally, a spectral mirror operation is conducted on the rotated data $\tilde{\mathbf{I}}^{\theta}$ to obtain the spectral mirroring data $\tilde{\mathbf{I}}^{\theta}$. After performing these data augmentation operations, the expanded training set is written as $\mathbf{X} = \left\{\tilde{\mathbf{I}}^{\theta} \cup \tilde{\mathbf{I}}_1^{\theta}\right\}$. During the training stage, we randomly select an augmented image from $\mathbf{X}$ as the input of the deep network.

2.2 Self-supervised feature learning

After data augmentation, we need to learn more discriminant representations from the input cube without any class label information. Many advanced CNN models, showing outstanding performance in classification tasks, can be considered as the backbone, such as VGGNet, GoogleNet, and ResNet. Nevertheless, the deeper neural networks, the higher the computing complexity. With this consideration in mind, ResNet 50 is used as backbone architecture to generate the feature embedding of the input hyperspectral cube since it makes a good balance between feature characterization and time-consuming.

For each hyperspectral cube $\mathbf{x}_i$ which is cropped from a hyperspectral image with a certain size $W \times W$. Let $\mathcal{F}(\cdot, \varphi)$ be the encoder network which is a CNN parameterized by φ, $\mathbf{f}_i^m \in \mathbb{R}^D$ is the deep embedding of $\mathbf{x}_i^m$ obtained by the CNN model, where D denotes the feature dimension. For self-supervised learning, given the unlabelled training sample $\mathbf{x}_i^m$ and its augmented version $\mathbf{x}_i^n$, $\mathbf{f}_i^m$ and $\mathbf{f}_i^n$ are the embedding vectors of the training samples $\mathbf{x}_i^m$ and $\mathbf{x}_i^n$, respectively. To train the encoder, the main idea is to make similar samples closer and dissimilar samples far from each other. One common technique to solve this problem is that a similarity

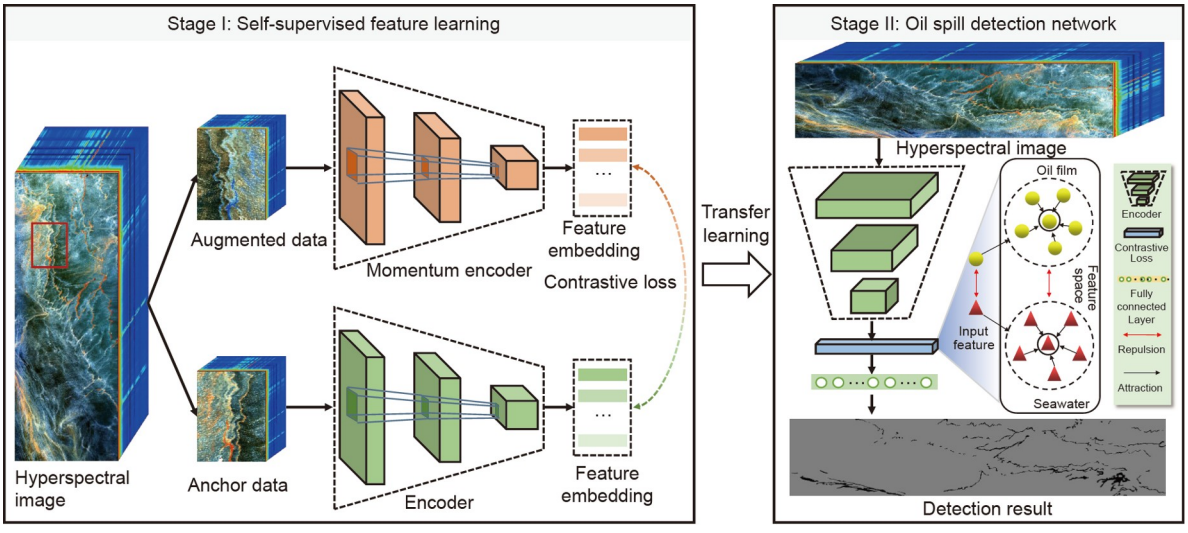

Figure 1 Schematic diagram of the proposed self-supervised learning model.

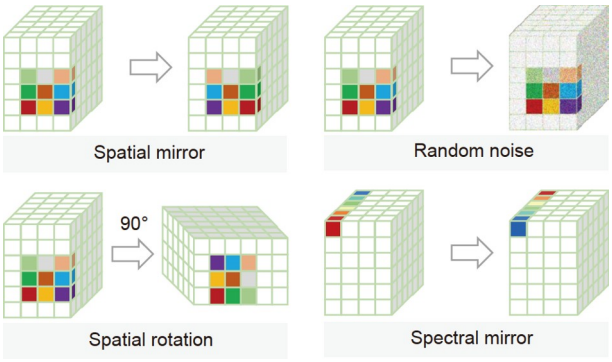

Figure 2 Spectral and spatial image transformation-based data augmentation technique.

criterion is used to measure the affinity between the embedding of two samples. In this work, a contrastive learning strategy [26] is adopted, where the contrastive loss of $\mathbf{x}_i^m$ is expressed as

$$L_i = -\log \frac{\exp\left(\left\langle \mathbf{f}_i^m, \mathbf{f}_i^n \right\rangle / \tau\right)}{\sum_{j=1}^{M} \exp\left(\left\langle \mathbf{f}_i^m, \mathbf{f}_j^m \right\rangle / \tau\right)}. \tag{1}$$

Here, inner product operation $\langle \mathbf{f}_i^m, \mathbf{f}_i^n \rangle$ is to calculate the similarities between a pair of feature embedding vectors in the projection space. τ stands for a temperature parameter. The contrastive loss acts as an unsupervised energy function for training the encoder network.

To fully learn the deep feature embedding with the CNN model, a scalable input dataset needs to be fed into the CNN. Moreover, for the larger batch size, this model easily suffers from a large mini-batch optimization issue during training. To alleviate this problem, a momentum bank mechanism [27] is adopted which is used to accumulate abundant feature representations, serving as negative samples. In more detail, a queue of the feature vectors of image cube $\mathbf{x}_j^m$ is created with the current mini-batch enqueued and the oldest mini-batch dequeued. In the training stage, the embeddings of current mini-batch are compared with the ones in the queue. To consistently update the feature vectors in the queue, the momentum encoder model with parameters φ_{mo} is introduced. The update rule for momentum encoder is expressed as

$$\varphi_{mo}^{(t+1)} \leftarrow \lambda \varphi_{mo}^{(t)} + (1-\lambda)\varphi^{(t)}, \tag{2}$$

where $\lambda \in [0, 1)$ is the momentum coefficient. It should be mentioned that only the parameters φ are updated by means of backpropagation. The momentum update enables parameters φ_{mo} evolve more smoothly than φ.

2.3 Oil spill detection network

The oil spill detection network is to train a CNN classifier by making use of the pre-trained deep embedding obtained by self-supervised feature learning. First, the pre-trained CNN is performed on the training samples to obtain the corresponding deep features of each sample, and the deep features are used to build a dynamic feature store $\mathbf{F}_{\text{store}} = \{\mathbf{q}_0, \mathbf{q}_1\}$ that stores the class specific features in the corresponding queues. This feature store is updated as training, and the size of the queue is set as 20 for each class in this work. Then, for each known class i, we calculate the mean of feature vectors belonging to each class so as to construct the set of class prototypes: $\mathbf{P} = \{\mathbf{p}_0, \mathbf{p}_1\}$. The class prototypes gradually evolve as the constituent features change. Finally, we introduce a loss function [28] to fine-tune the feature extraction ability of the pre-trained network. Specifically, a prototype vector $\mathbf{p}_i$ for each known class i is selected from $\mathbf{P}$. Assume $\mathbf{f}_c \in R^d$ be a feature vector that is produced by the pre-trained network without projection head for class c. The contrastive loss is defined as follows:

$$L_{\text{cont}}(\mathbf{f}_c) = \sum_{i=0}^{C} \xi(\mathbf{f}_c, \mathbf{p}_i), \tag{3}$$

where

$$\xi(\mathbf{f}_c, \mathbf{p}_i) = \begin{cases} D(\mathbf{f}_c, \mathbf{p}_i), & i = c, \\ \max\{0, 1 - D(\mathbf{f}_c, \mathbf{p}_i)\}, & \text{otherwise.} \end{cases} \tag{4}$$

Here, D is spectral distance function. This loss is helpful to obtain the desired class discrimination in the feature space.

3 Experiment and result

3.1 Datasets

To validate the detection performance of different hyperspectral oil spill detection techniques, a benchmark dataset, i.e., hyperspectral oil spill detection database (HOSD), is used, which consists of 10 hyperspectral oil datasets collected from different flight paths at different altitudes. All images are captured with the AVIRIS sensor embedded on the unmanned aerial vehicle (UAV) aircraft. This sensor records 224 spectral channels with wavelength from 380 to 2500 nm. The spectral resolution is 5 nm. The study region is located in the Gulf of Mexico, North American continent (see Figure 3). This is the biggest marine oil spill accident in the US, which resulted in more than 200 million gallons of crude oils into the Gulf of Mexico. The specific details of the used database are given in Table 1. The pseudo color image of each hyperspectral oil dataset is shown in Figures 4 and 5.

3.2 Experimental setup

Parameter setting All deep networks considered in this work are simulated by PyTorch on Python3.6, running on a personal computer with Ubuntu20.04, NVIDIA GeForce RTX 2080Ti and Intel(R) Core(TM) i9-9900K CPU @ 3.60

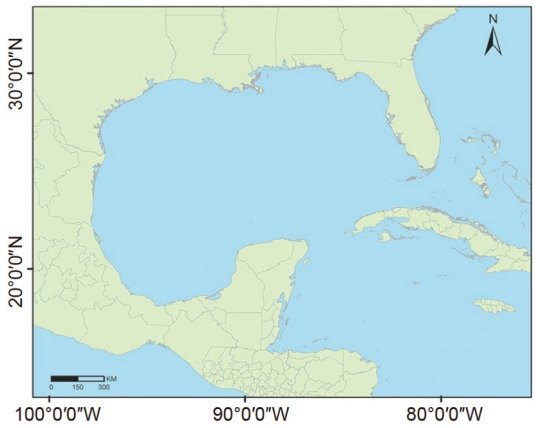

Figure 3 Study area.

Table 1 The specific details of the oil spill detection database

Datasets	Spatial resolution (m)	Spatial size (pixel)
GM01	7.6	1243×684
GM02	3.3	1965×492
GM03	7.6	1386×690
GM04	7.6	1466×676
GM05	7.6	2085×682
GM06	8.1	2088×691
GM07	3.2	1569×517
GM08	7.6	1185×682
GM09	7.6	842×640
GM10	3.2	836×572

GHz. The spatial window of each cropped cube is set to be 11. SGD is used to optimize the networks, and the batch size is set as 256. In the self-supervised feature learning phase, the maximum training epoch is set to be 200, and the learning rate is set to be 0.03. When the epoch reaches 120 and 160, the current learning rate is updated by multiplying 0.1. In the oil spill detection phase, the maximum training epoch is set to be 100, and the learning rate of the proposed method is set to be 0.00001. When the epoch reaches 60 and 80, the learning rate can be updated by multiplying 0.1. In addition, 10 % labelled samples selected from GM 01 and GM 02 datasets are used to train the CNN classifier and the other datasets are used to test the detection performance.

Compared methods To evaluate the effectiveness of the proposed method, several state-of-the-art hyperspectral detection approaches are adopted as competitors, including 3DCNN [29], momentum contrast (MOCO) [27], rank-two nonnegative matrix factorization (R2NMF) [30], low-rank and sparse matrix decomposition (LRSMD) [31], and kernel isolation forest (KIF) [32]. For all compared methods, we follow the default parameters in the corresponding publications. The source code of the proposed method will be released online at the author's Github repository[1)].

Objective index In order to quantitatively assess the detection accuracy of all considered approaches, a widely used objective index [33], i.e., area under curve (AUC), is used. Given the detection result and reference label, the AUC can be expressed as

$$\mathrm{AUC} = \int_{-\infty}^{+\infty} \mathrm{TPR}(H)\mathrm{FPR}'(H)\mathrm{d}H, \tag{5}$$

where the true positive rate TPR(H) calculates what proportion of the positive samples got correctly identified by the proposed method when the threshold is H. The false positive rate FPR(H) indicates what proportion of the negative samples got correctly detected by the proposed model. The higher the AUC, the better the performance of this method at distinguishing between the positive and negative samples.

3.3 Component analysis

Here, the effects of two key steps, i.e., the data augmentation and contrastive loss, to the detection accuracy of the proposed method are analysed. The experiment is conducted on the HOSD database. Table 2 gives the detection accuracy of the proposed method with or without the two key steps. As shown in Table 2, the proposed method without contrastive loss obtains the lowest detection accuracy in terms of the averaged AUC, and the AUC for different hyperspectral datasets shows severe fluctuations, which demonstrates that the proposed method without contrastive loss has poor generalization capability. After the contrastive loss is introduced in the oil spill detection network, the AUC obtained by the proposed method is increased by 8.59% on average with respect to the proposed method without the contrastive loss, which demonstrates that this step is beneficial for improving generalization of the proposed model.

Furthermore, it is found that the proposed method without the data augmentation step tends to decrease the detection accuracy. By comparing the AUC for different hyperspectral datasets, when the data augmentation is not used in the proposed method, the detection accuracy of the proposed method tends to decrease on the HOSD database. The main reason is that the data augmentation can effectively increase the robustness of the extracted features. Moreover, the proposed method yields the highest detection accuracy among three methods, which illustrates that both data augmentation and contrastive loss make important contributions for oil spill detection. This experiment also confirms the effectiveness of the data augmentation and the contrastive loss steps to the proposed method.

1) https://github.com/PuhongDuan

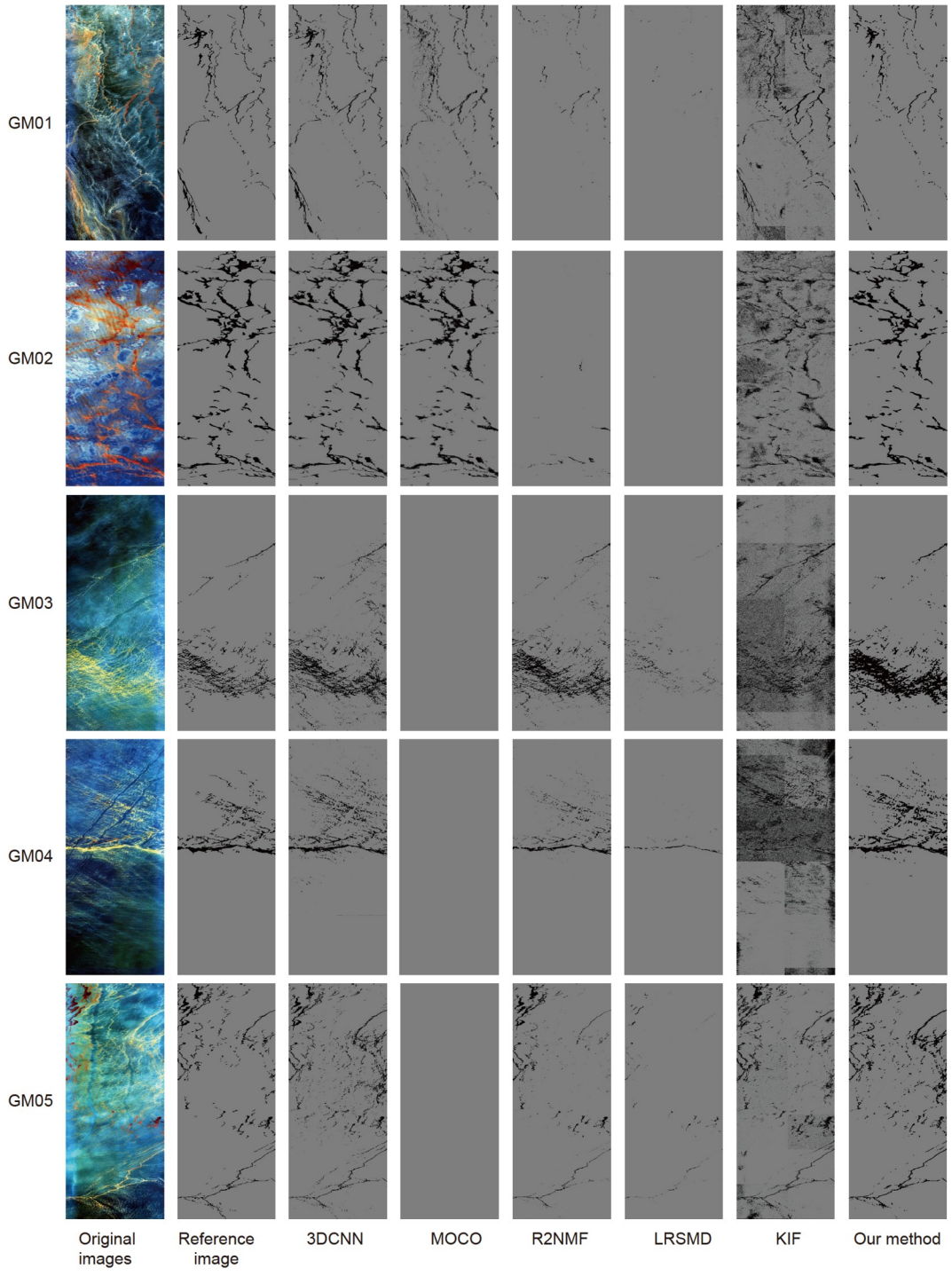

Figure 4 The detection maps of different methods on GM01-GM05.

3.4 Experimental results

Table 2 lists the objective results of all methods on the HOSD database. The objective accuracy obtained by 3DCNN method exceeds that of the proposed method on GM 01 and GM 02. This is because the 3DCNN method is a supervised detection method, which makes full use of the class label information. The MOCO model cannot work well for hyperspectral oil spill detection. The detection accuracy obtained by the MOCO model is relatively low. This is due to the fact that this model freezes the weights of the pre-trained feature extractor when it trains the detection network. The R2NMF method improves the detection accuracy with respect to the MOCO model. However, the detection accuracies on some datasets are still unsatisfactory. Similarly, the LRSMD method also yields a low objective accuracy.

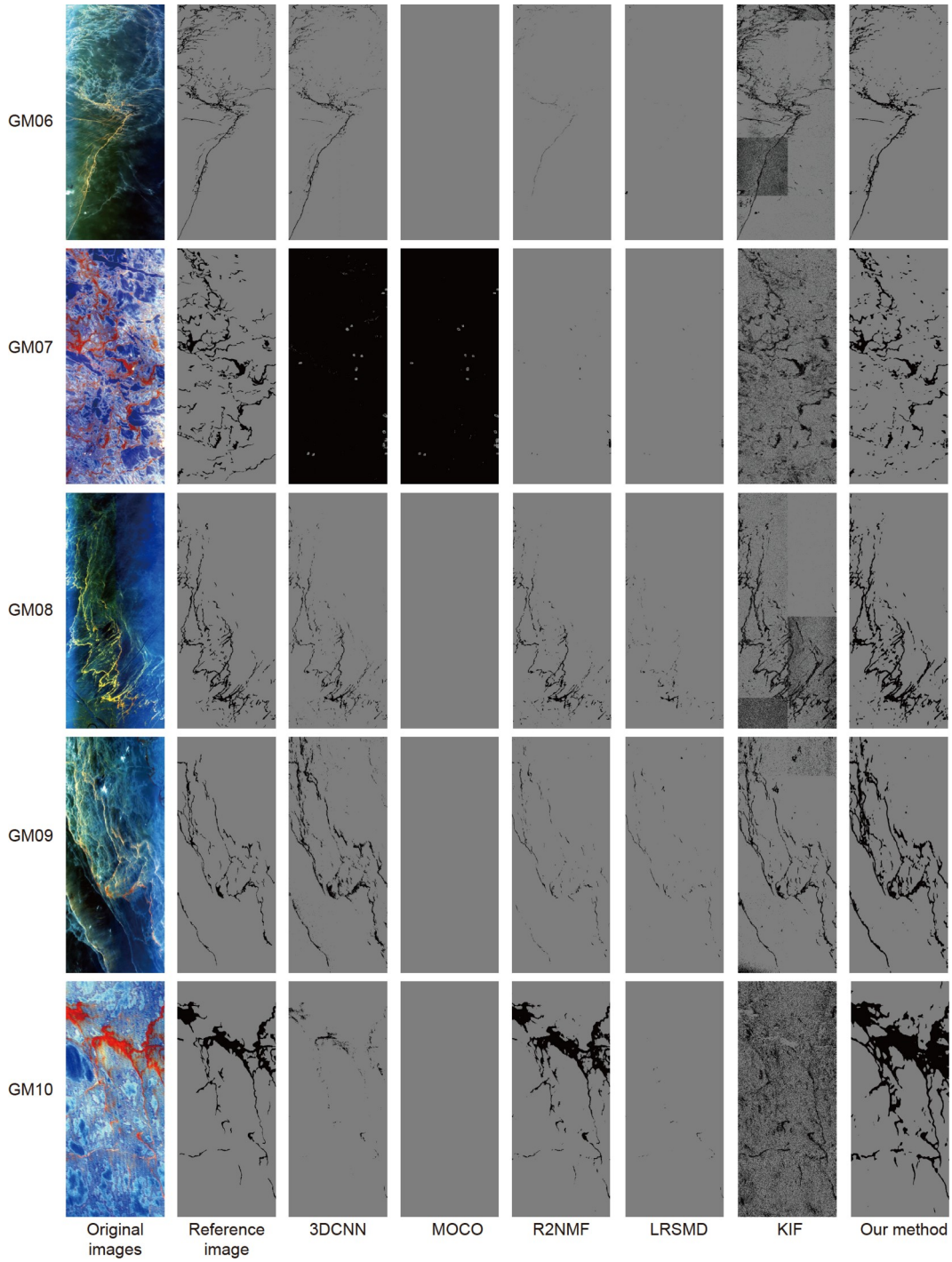

Figure 5 The detection maps of different methods on GM06-GM10.

The KIF method shows great improvement compared with other competitors. Nevertheless, it also has poor detection accuracy on few datasets, such as GM 02 and GM 10. Different from other methods, the proposed method obtains the highest detection accuracy among all considered approaches, and works well on all hyperspectral datasets. The main reason is that the pre-trained feature extraction and fine-tuning steps make a great contribution to oil spill detection, which enhances the transfer ability of the proposed model.

Figures 4 and 5 show the detection maps of different methods. By observing these resulting images, it can be seen that the 3DCNN method can detect the oil spill regions on most of hyperspectral images. However, it cannot work well such as GM 07 and GM 10 datasets due to low robustness. The detection results obtained by the MOCO method are unsatisfactory. The reason is that the MOCO method freezes

Table 2 AUC values of different hyperspectral oil spill detection approaches

Datasets	Detection accuracies of different detection methods							
	3DCNN [23]	MOCO [22]	R2NMF [24]	LRSMD [25]	KIF [26]	Our method without loss	Our method without augmentation	Our method
GM01	**0.8845**	0.7048	0.5578	0.5073	0.8109	0.7802	0.7403	0.7703
GM02	**0.9163**	0.8702	0.5131	0.4999	0.6966	0.8964	0.8833	0.8783
GM03	0.8885	0.5000	0.9395	0.5809	0.7720	0.9108	0.9444	**0.9463**
GM04	0.8797	0.5000	0.7505	0.5407	0.7249	0.4995	0.7957	**0.9514**
GM05	0.8545	0.5000	0.7734	0.5413	0.8483	**0.9185**	0.8332	**0.9018**
GM06	0.7102	0.5000	0.5258	0.5014	**0.8534**	**0.9238**	0.7211	0.8280
GM07	0.5009	0.5002	0.5001	0.4997	0.7223	**0.9244**	0.8823	**0.8688**
GM08	0.7411	0.5000	0.7732	0.5521	0.8642	0.9478	0.9570	**0.9656**
GM09	0.8598	0.5000	0.6385	0.5605	0.8953	0.9494	0.9646	**0.9623**
GM10	0.5597	0.5000	0.9671	0.5041	0.5350	0.5496	0.9297	**0.9411**
Mean	0.7795	0.5575	0.6939	0.5288	0.7723	0.8300	0.8652	**0.9014**

the features when training supervised linear classifier, and thus, this method has a low generalization. The R2NMF method only works on few hyperspectral images due to the spectral similarity between the can seawater. The LRSMD method presents poor detection results since the Mahalanobis distance in the LRSMD cannot well model the separability between the seawater and oil film. Although the KIF method can detect the oil spill regions, the detection maps have serious noisy labels. As can be seen, the proposed method exhibits the best performance for oil spill detection. The oil spill regions can be well identified on all datasets, which also illustrates the strong generalization ability of the extracted deep features.

4 Conclusions

In this study, we propose a self-supervised learning method for hyperspectral oil spill detection, which is composed of three steps. First, a spectral and spatial transformation technique is used to augment the input data so as to enhance the robustness of the proposed method. Then, the CNN encoder is trained to extract the deep semantic features from the input cube and its augmented data, and this step does not require the involvement of manually annotated labels. Finally, the pre-trained CNN parameters are transferred into the CNN classifier to decrease the labelled sample usage and avoid the overfitting of the training model. Experiments on the HOSD database verify the effectiveness of the proposed method, and several main conclusions can be obtained as follows: (1) The self-supervised learning exhibits huge potentials for hyperspectral oil spill detection. (2) The spectral similarity-based contrastive loss is helpful for increasing the generalization of the proposed model. (3) Experiments reveal that the proposed method yields the best detection performance with respect to other state-of-the-art detection approaches.

This work was supported by the National Natural Science Foundation of China (Grant No. 61890962 and 61871179), the Scientific Research Project of Hunan Education Department (Grant No. 19B105), the Natural Science Foundation of Hunan Province (Grant Nos. 2019JJ50036 and 2020GK2038), the National Key Research and Development Project (Grant No. 2021YFA0715203), the Hunan Provincial Natural Science Foundation for Distinguished Young Scholars (Grant No. 2021JJ022), and the Huxiang Young Talents Science and Technology Innovation Program (Grant No. 2020RC3013).

1 Wang X Z, Liu D, Cheng G, et al. Solar heating assisted rapid cleanup of viscous crude oil spills using reduced graphene oxide-coated sponges. Sci China Tech Sci, 2020, 63: 1487–1496
2 Gu Y F, Jin X D, Xiang R Z, et al. UAV-based integrated multi-spectral-LiDAR imaging system and data processing. Sci China Tech Sci, 2020, 63: 1293–1301
3 Qin F K, Chen S T, Chen R, et al. Leakage detection of oil tank using terahertz spectroscopy. Sci China Tech Sci, 2021, 64: 1947–1952
4 Duan P, Ghamisi P, Kang X, et al. Fusion of dual spatial information for hyperspectral image classification. IEEE Trans Geosci Remote Sens, 2021, 59: 7726–7738
5 Zhang S, Kang X, Duan P, et al. Polygon structure-guided hyperspectral image classification with single sample for strong geometric characteristics scenes. IEEE Trans Geosci Remote Sens, 2022, 60: 1–12
6 Kang X, Duan P, Xiang X, et al. Detection and correction of mislabeled training samples for hyperspectral image classification. IEEE Trans Geosci Remote Sens, 2018, 56: 5673–5686
7 Lu Y C, Shi J, Hu C M, et al. Optical interpretation of oil emulsions in the ocean. Part II: Applications to multi-band coarse-resolution imagery. Remote Sens Environ, 2020, 242: 111778
8 Pelta R, Carmon N, Ben-Dor E. A machine learning approach to detect crude oil contamination in a real scenario using hyperspectral remote sensing. Int J Appl Earth Observ GeoInf, 2019, 82: 101901
9 Yang J, Ren G, Ma Y, et al. Oil spill AISA+ hyperspectral data detection based on different sea surface glint suppression methods. Int Arch Photogramm Remote Sens Spatial Inf Sci, 2018, XLII-3: 2083–2087
10 Löw F, Stieglitz K, Diemar O. Terrestrial oil spill mapping using satellite earth observation and machine learning: A case study in South

Sudan. J Environ Manage, 2021, 298: 113424
11 Duan P, Lai J, Kang J, et al. Texture-aware total variation-based removal of sun glint in hyperspectral images. ISPRS J Photogram Remote Sens, 2020, 166: 359–372
12 Liu D, Han L. Spectral curve shape matching using derivatives in hyperspectral images. IEEE Geosci Remote Sens Lett, 2017, 14: 504–508
13 Liu D, Zhang J, Wang X. Reference spectral signature selection using density-based cluster for automatic oil spill detection in hyperspectral images. Opt Express, 2016, 24: 7411
14 Song D M, Liu B, Chen S C, et al. Classification of the different thickness of the oil film based on wavelet transform spectrum information. Aquat Procedia, 2015, 3: 133–143
15 Liu B, Li Y, Chen P, et al. Extraction of oil spill information using decision tree based minimum noise fraction transform. J Ind Soc Remote Sens, 2016, 44: 421–426
16 Song M P, Chang M, An J B, et al. Active contour segmentation for hyperspectral oil spill remote sensing. In: Proceedings of the Society of Photo-Optical Instrumentation Engineers (SPIE) Conference Series. Beijing, 2013. 891026
17 Wang B, Shao Q, Song D, et al. A spectral-spatial features integrated network for hyperspectral detection of marine oil spill. Remote Sens, 2021, 13: 1568
18 Zhu X, Li Y, Zhang Q, et al. Oil film classification using deep learning-based hyperspectral remote sensing technology. Int J Geo-Infor, 2019, 8: 181
19 Yang J F, Wan J H, Ma Y, et al. Oil spill hyperspectral remote sensing detection based on DCNN with multi-scale features. J Coast Res, 2019, 90: 332
20 Lan M, Zhang Y, Zhang L, et al. Global context based automatic road segmentation via dilated convolutional neural network. Inf Sci, 2020, 535: 156–171
21 Sun X, Qu Y, Gao L, et al. Target detection through tree-structured encoding for hyperspectral images. IEEE Trans Geosci Remote Sens, 2021, 59: 4233–4249
22 Yue J, Fang L, Rahmani H, et al. Self-supervised learning with adaptive distillation for hyperspectral image classification. IEEE Trans Geosci Remote Sens, 2022, 60: 1–13
23 Hong D, Gao L, Yao J, et al. Graph convolutional networks for hyperspectral image classification. IEEE Trans Geosci Remote Sens, 2021, 59: 5966–5978
24 Zheng K, Gao L, Liao W, et al. Coupled convolutional neural network with adaptive response function learning for unsupervised hyperspectral super resolution. IEEE Trans Geosci Remote Sens, 2021, 59: 2487–2502
25 Hong D, Gao L, Yokoya N, et al. More diverse means better: multimodal deep learning meets remote-sensing imagery classification. IEEE Trans Geosci Remote Sens, 2021, 59: 4340–4354
26 Oord van den A, Li Y, Vinyals O. Representation learning with contrastive predictive coding. arXiv: 1807.03748
27 He K, Fan H, Wu Y, et al. Momentum contrast for unsupervised visual representation learning. arXiv: 1911.05722
28 Joseph K J, Khan S, Khan F S, et al. Towards open world object detection. In: Proceedings of the IEEE Conference Comput Vis Pattern Recognit. Nashville, 2021. 5826–5836
29 Ben Hamida A, Benoit A, Lambert P, et al. 3-D deep learning approach for remote sensing image classification. IEEE Trans Geosci Remote Sens, 2018, 56: 4420–4434
30 Gillis N, Kuang D, Park H. Hierarchical clustering of hyperspectral images using rank-two nonnegative matrix factorization. IEEE Trans Geosci Remote Sens, 2015, 53: 2066–2078
31 Zhang Y, Du B, Zhang L, et al. A low-rank and sparse matrix decomposition-based mahalanobis distance method for hyperspectral anomaly detection. IEEE Trans Geosci Remote Sens, 2016, 54: 1376–1389
32 Li S, Zhang K, Duan P, et al. Hyperspectral anomaly detection with kernel isolation forest. IEEE Trans Geosci Remote Sens, 2020, 58: 319–329
33 Fawcett T. An introduction to ROC analysis. Pattern Recognit Lett, 2006, 27: 861–874